Interaction of an Ultrarelativistic Electron Bunch Train with a *W*-Band Accelerating Structure: High Power and High Gradient

D. Wang,[1,2,*] S. Antipov,[1,3,†] C. Jing,[1,3] J. G. Power,[1] M. Conde,[1] E. Wisniewski,[1] W. Liu,[1] J. Qiu,[1,3] G. Ha,[1] V. Dolgashev,[4] C. Tang,[2] and W. Gai[1]

[1]*High Energy Physics Division, Argonne National Laboratory, Lemont, Illinois 60439, USA*
[2]*Tsinghua University, Beijing, 100084, China*
[3]*Euclid Techlabs LLC, Solon, Ohio 44139, USA*
[4]*SLAC National Accelerator Laboratory, Menlo Park, California 94025, USA*

(Received 6 October 2015; published 5 February 2016)

Electron beam interaction with high frequency structures (beyond microwave regime) has a great impact on future high energy frontier machines. We report on the generation of multimegawatt pulsed rf power at 91 GHz in a planar metallic accelerating structure driven by an ultrarelativistic electron bunch train. This slow-wave wakefield device can also be used for high gradient acceleration of electrons with a stable rf phase and amplitude which are controlled by manipulation of the bunch train. To achieve precise control of the rf pulse properties, a two-beam wakefield interferometry method was developed in which the rf pulse, due to the interference of the wakefields from the two bunches, was measured as a function of bunch separation. Measurements of the energy change of a trailing electron bunch as a function of the bunch separation confirmed the interferometry method.

DOI: 10.1103/PhysRevLett.116.054801

Cost and power consumption of microwave electron accelerators become prohibitive for the next energy frontier machines which require a multi-TeV level collision energy [1,2]. Advanced accelerator concepts [3–5] capable of high acceleration gradients are under study to reduce the footprint of such machines. Accelerators working at a higher frequency (millimeter wave and beyond) [6,7] are good candidates to achieve a much higher gradient because: (i) the accelerating gradient increases with frequency at a fixed power; (ii) a shorter rf pulse is affordable for high frequency accelerating structures and, thus, helps achieve a stable high gradient [8–10]. While vacuum tube technology [11–15] for driving high frequency structures is under development, beam-driven devices use wakefields from a high charge drive bunch (or bunch train) to generate rf pulses with stable a phase and amplitude necessary to accelerate a witness beam in both the collinear acceleration [16] and the two beam acceleration schemes [17]. Benefiting from the short rf pulse and high gradient, the high frequency wakefield acceleration is also attractive in the application of high repetition rate (MHz level) free electron lasers (FELs) [18].

In this Letter, we report on the generation of high-power rf with precise phase and amplitude control in a W-band ($f_0 = 91$ GHz, $\lambda_0 = 3.3$ mm) planar accelerating structure driven by a variable separation four-bunch train. The individual rf pulse ("rf pulse" and "wakefield" are used interchangeably in this Letter) generated by a single bunch are due to the interaction of the structure's electromagnetic (EM) modes with the EM fields of the bunch [19,20], and the total rf pulse generated by the bunch train is the superposition of the individual rf pulses. The rf pulse generated by a single bunch typically has a pulse width of a few nanoseconds as determined by the structure's group velocity and length. The interference of the individual rf pulses can be varied by changing the bunch separation resulting in both constructive and destructive interference, thus, providing a means to tailor the total rf pulse.

The experiment was performed at the Argonne Wakefield Acceleration Facility at Argonne National Laboratory [21]. Figure 1 shows the layout of the experiment.

There are a number of methods for producing a bunch train: transverse-to-longitudinal phase-space exchange in combination with a multislit mask [22,23], self-energy modulation followed by chicane compression [24], and others. In our experiment, the bunch train was generated directly from a rf photoinjector illuminated by a series of laser pulses with variable spacing to provide a tunable drive bunch train and witness bunch [25]. The electron bunch train has the same time structure as the laser pulse train. The laser train was variable from 1 to 4 pulses with a nominal bunch separation of $z_0 = 230$ mm in order to be synchronous with the 1.3 GHz rf photoinjector and accelerating cavities. In addition, the laser separation was tunable ± 3 mm around z_0 so that the entire 91 GHz period could be swept.

A 65 MeV electron bunch train was used to excite the W-band structure. The train from the linac was focused with quadrupoles, and its trajectory was adjusted with trim magnets to pass it through the center of the W-band structure. The charge of a single bunch in the train was varied from 0.1 nC to 4 nC during the experiment. Each bunch had a

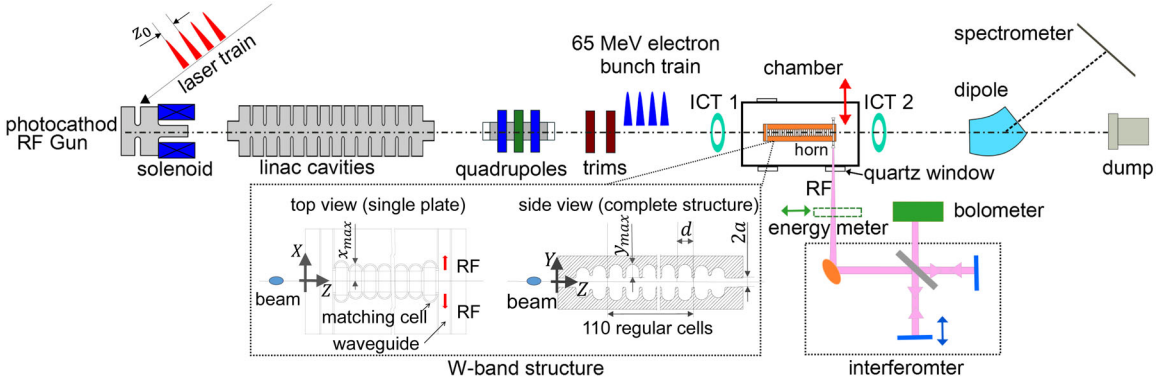

FIG. 1. Schematic of the experimental setup.

longitudinal Gaussian distribution and corresponding rms bunch length of 0.2 to 0.6 mm. Note, the longer bunch lengths at higher charge are due to stronger space charge effects. The integrating current transformers (ICT 1 and ICT 2) were used to record the charge of the drive beam before and after the W-band structure, respectively, to determine the percentage of charge transmitted.

The W-band planar accelerating structure (Fig. 1, inset) consists of two identical copper plates with periodic grooves separated by a vertical gap $= 2a$. It is a $2\pi/3$ mode traveling wave structure of length 123 mm [26]. The rf pulse excited by the electron bunch propagates in the same direction as the beam and is coupled out of the structure through a matching cell and perpendicular waveguide fitted with standard gain WR10 horn antennas. The vertical gap was adjusted to generate wakefields at 91 GHz (a harmonic of 1.3 GHz). The structure was installed on a motorized actuator inside a vacuum chamber. A local reference laser was available for structure alignment to the electron beam trajectory. Structure parameters are summarized in Table I.

The rf pulse extracted from the accelerating structure was characterized by two direct methods and one indirect method. The rf pulse exited the structure through the WR10 horn antenna, passed through a quartz window mounted on the vacuum chamber, and propagated into the detection system. A calibrated photoacoustic energy meter [27] was used to measure the rf pulse energy and a Michelson interferometer with a helium-cooled bolometer was used to measure the time domain characteristics of the rf pulse. In addition to the direct measurements of the rf pulse, the kinetic energy of the electron bunches was measured with a spectrometer to indirectly characterize the wake since the electron bunches lose energy to generate the wakefield. Taken together, these methods were used to characterize the interaction of various bunch trains with the W-band wakefield structure.

TABLE I. Parameters of the W-band structure in Fig. 1.

Parameter	Value	Unit	Description
f_0	91.0	GHz	Frequency of the fundamental mode
$2a$	0.94	mm	Gap between the two plates
d	1.10	mm	Length of the regular cell
$x_{\max}$	1.25	mm	Half width of the regular cell
$y_{\max}$	0.90	mm	Depth of the regular cell
L_s	123.20	mm	Total length of the grooved structure
β_g	0.105		Relativistic group velocity
Q	2560.0		Total quality factor
R/Q	83.3	$k\Omega/m$	R over Q per unit length
α	3.55	$1/m$	Field attenuation per unit length

The fundamental frequency (f_0) and bandwidth (BW) of the structure were measured with an interferometric autocorrelation of the wakefield signal produced by a single electron bunch. The simulated values are $f_0 = 91$ GHz and, given the single rf pulse width, $\tau = L_s(1/\beta_g c - 1/c) = 3.4$ ns (c is the speed of light), BW $= 1/\tau = 0.3$ GHz. Because of the limited travel range of the interferometer, the experimental data (integrated signal intensity as a function of interferometer mirror position) shown in Fig. 2(a), is only a small fraction (19 mm) of the full rf pulse width in air ($\tau c = 1019$ mm). Taking an FFT of the measured data yields a center frequency of 91.3 GHz (in good agreement with simulation) and BW $= 13.1$ GHz as shown in Fig. 2(b) (broader due to the limited range of the interferometer).

The rf pulse energy as a function of beam charge was measured with a calibrated meter (Fig. 1) and compared to simulation. The electromagnetic code CST [28] was used to simulate the rf energy generated by the beam with rf losses (structure attenuation) included. The rf power depends on the electron bunch parameters according to $P \propto Q_b^2 F(\sigma_z)$ [25], where Q_b is the single bunch charge and $F(\sigma_z)$ is the bunch form factor (Fourier transform of the normalized charge density distribution). To estimate σ_z as a function of Q_b, the beam dynamics code ASTRA [29] was used for start to end beam line simulations to determine the electron beam parameters in the W-band structure. This showed that σ_z increases with Q_b due to space charge effects which results in the reduction of the form factor and, therefore, slower power growth with charge than would occur if σ_z

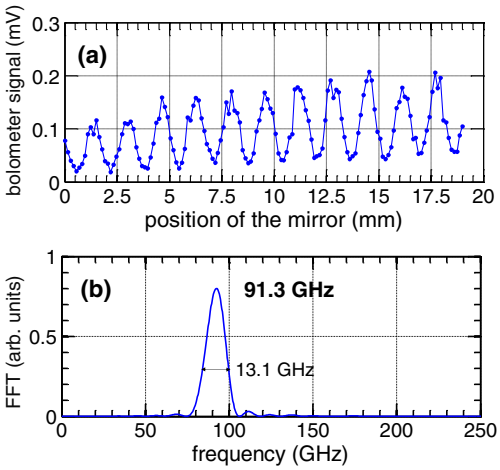

FIG. 2. rf frequency measurement with the interferometer.

were constant. The "effective charge" contributing to the rf power generated is bounded between the incident charge measured before (ICT 1) and the transmitted after (ICT 2) the structure. Figure 3(a) shows the upper and lower limits of the rf power due to the respective charges. The effective charge fit to the measured rf energy data was about 2/3 of the charge at ICT 1.

The energy distribution of a drive bunch was measured both with and without the structure present [solid lines in Fig. 3(b)] and used to confirm the effective charge estimate given above. The energy lost by the drive bunch depends on its charge which, as before, is bounded between the charge measured at ICT 1 (3 nC) and ICT 2 (1 nC). Simulations of average energy changes of 1 and 3 nC bunches passing through the structure are −0.7 and −2 MeV, respectively [Fig. 3(b)]. An effective charge of 2 nC [Gaussian beam with $F(\sigma_z = 0.5\ \text{mm}) = 0.4$)] provides the best fit to the measured energy distribution and agrees well with the estimate of the effective charge obtained by the rf energy measurements. Because of the imperfections of beam alignment and focusing, part of the bunch may have been lost at the entrance or inside the structure, which means no contribution or only a partial contribution to the rf radiation. The effective charge is used to describe the effective contribution from the drive beam on average.

The energy and the amplitude of the rf pulse generated by the two-bunch drive train depends on the bunch separation. Consider two bunches traversing the structure: each bunch generates a wakefield and the total energy in the rf pulse depends on how these two wakes interfere. The energy will vary between minimum and maximum as the delay of the trailing bunch is scanned [Fig. 4(a)] with the cycle repeating at the rf wavelength, 3.3 mm. Simulated rf pulse envelopes in Fig. 4(a) correspond to the energy measurements in cases (1)–(4), which also show the modulations of the rf pulse amplitude. In case (1), the individual wakes add constructively, generating the maximum rf energy. In case (3), however, the wake of the trailing bunch interferes destructively, so the output rf energy is minimal, which does not drop completely to zero since the rf pulses don't fully overlap in time due to bunch separation.

The energy change of the trailing bunch also depends on the bunch separation [Fig. 4(b)]. (Note, the leading bunch loses the same energy regardless of the position of the trailing bunch since its wake doesn't affect the leading bunch.) In case (1), the trailing bunch gets decelerated by the wake from the leading bunch. It losses more energy than the leading bunch and contributes to the maximum rf amplitude. In case (3), however, the trailing bunch rides on the acceleration phase so that it gains energy from the wake of the leading bunch. Energy measurements of the two bunches are consistent with the rf envelope descriptions in cases (1) and (3). The inconsistencies between the measurements and the simulations in Fig. 4(b) are due to the differences between the average effective charge in the simulations (100% transmission) and the complicated particle loss process in reality. This measurement is equivalent to wakefield mapping [30,31] where the energy change of a trailing bunch is measured with a spectrometer as a function of its delay behind the leading bunch.

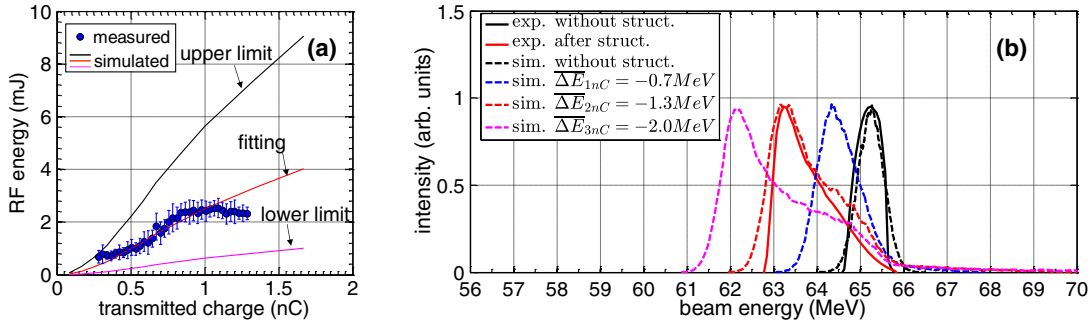

FIG. 3. Comparison of measurements and simulations of (a) rf energy versus transmitted charge measured with ICT 2. The upper limit of the rf energy is calculated using the incident charge measured before the entrance of W-band structure, and the lower limit is calculated using the charge measured at the exit. (b) The energy distributions with and without the presence of the W-band structure for fixed charge (ICT 1 = 3 nC, ICT 2 = 1 nC).

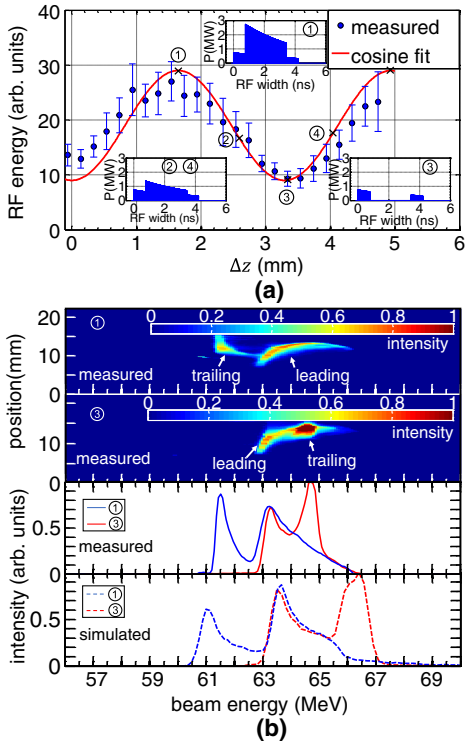

FIG. 4. (a) Measured rf energy vs the change in bunch separation, $\Delta z \equiv z - z_0$, which fits a 3.3 mm wavelength cosine function (z_0 is the nominal bunch separation). Labels (1)–(4) correspond to different relative wakefield phases when the leading bunch and the trailing bunch add. The simulated rf pulse power envelope in cases (1)–(4) are also shown in the figure. (b) Comparison between the simulations and experimental observations of the energy distributions of two bunches after the W-band structure. In case (1), the trailing bunch was decelerated by the wakefield from the leading bunch; in case (3), the trailing bunch was accelerated.

Proper bunch spacing was set and rf wavelength was measured with a newly developed two-beam (wakefield) interferometry method based on the energy of the rf pulse described above. Two-beam interferometry (based on rf pulse energy) can be used for these two purposes for lower charge trains than traditional wakefield mapping (based on trailing bunch energy loss) for two reasons: (i) interferometry does not depend on bunch energy spread and energy jitter, and (ii) the relative energy loss due to the wakefield of a low charge bunch is often small (e.g., 100 pC loses ~70 keV out of 65 MeV in this experiment) and, therefore, difficult to measure. In contrast, the energy of the rf pulse generated by the same charge (100 pC) is on the order of 7 μJ, which can be easily measured with a bolometer (~nJ sensitivity). In fact, this measurement only requires an integrating energy meter, such as a Golay cell, pyroelectric detector, bolometer, or diode detector. In general, two-beam interferometry can be used for tuning drive bunch train separation for wakefield accelerators [32–34] and microbunch trains for FELs [23,35].

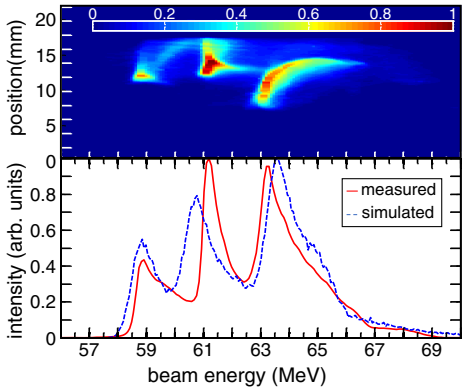

FIG. 5. Energy spectrometer measurements of the bunch train passing through the W-band structure, compared with the simulation results on three bunches of a 2 nC (effective charge) drive beam passing through the structure, with the wakefields adding up in phase.

The duration of the rf pulse excited by a single bunch is finite ($\tau = 3.4$ ns, in this case), so that the total number of bunches that can constructively overlap is ceiling $(\tau/T_b) - 1$, where T_b is the bunch spacing. A train of bunches beyond this number will increase the final rf pulse length, but not the rf power [25]. The saturated rf output power generated in the experiment was with a train of four bunches. The highest power corresponds to the case when all bunches lose energy to the wake. In the original bunch train, each bunch had approximately the same energy distribution [black solid line shown in Fig. 3(b)]. The measured energy distribution of the bunch train after traversing the W-band structure is shown in Fig. 5. Three bunches with different energy losses are clearly visible but the fourth bunch is missing. The missing bunch is not fully understood but was likely caused by a combination of two effects. First, the energy balance from the laser multisplitter resulted in a low-charge fourth bunch (15% of bunch 1) so that it contributed less to the power of the rf pulse. Second, the transverse wakefield may have kicked the beam out of the structure after only a very short distance so that it, again, contributed less to the wakefield. For the following analysis, we assumed no contribution from the fourth bunch. The blue dashed line in Fig. 5 gives the simulated energy spectrum of three bunches, each of 2 nC effective charge, passing through the W-band structure. These agree well with the experimental observation on the spectrometer. The average energy loss of bunch 1 through 3 was 1.3, 3.2, and 4.4 MeV, respectively, indicating coherent superposition of wakefields for maximum radiated power. Given the energy meter measurement of 18 mJ per pulse, we calculate the maximum peak power of 4.8 MW (in agreement with the simulation of a 3×2 nC bunch train) and peak accelerating gradient of 85 MV/m. Simulations show that, with an optimized beam line optics setup, the beam transmission through the structure can be improved to 5 nC per bunch which leads to 70 MW rf

output. This indicates that, with improved beam quality, a similar structure could be used for high-gradient wakefield acceleration [16,26].

In summary, a W-band wakefield accelerating structure driven by a bunch train was experimentally characterized. A two-beam wakefield interferometry measurement was developed as a high sensitivity technique for wakefield characterization and precise rf phase control in wakefield acceleration. A 5 MW rf pulse was generated corresponding to an accelerating gradient of 85 MV/m.

The authors would like to thank S. Doran, C. Whiteford, T. Benseman, and Y. Hao from ANL, Piot from FNAL for help on the experiment. Euclid Techlabs acknowledges support from DOE SBIR Grant No. DE-SC0009571. The Argonne Wakefield Accelerator Facility is supported by DOE Contract No. W-31-109-ENG-38.

*wangdan11@mails.tsinghua.edu.cn
†s.antipov@euclidtechlabs.com

[1] T. Behnke, J. E. Brau, B. Foster, J. Fuster, M. Harrison, J. M. Paterson, M. Peskin, M. Stanitzki, N. Walker, and H. Yamamoto, arXiv:1306.6327.
[2] T. Raubenheimer, H. Trautner, F. Perriollat, G. Carron, P. Pearce, J. Godot, D. Schulte, P. Royer, S. Döbert, R. Bossart *et al.*, CERN Report No. CERN-2000-008, 2000 (unpublished).
[3] I. Blumenfeld, C. E. Clayton, F.-J. Decker, M. J. Hogan, C. Huang, R. Ischebeck, R. Iverson, C. Joshi, T. Katsouleas, N. Kirby, W. Lu, K. A. Marsh, W. B. Mori, P. Muggli, E. Oz, R. H. Siemann, D. Walz, and M. Zhou, Nature (London) **445**, 741 (2007).
[4] W. P. Leemans, B. Nagler, A. J. Gonsalves, C. Toth, K. Nakamura, C. G. R. Geddes, E. Esarey, C. B. Schroeder, and S. M. Hooker, Nat. Phys. **2**, 696 (2006).
[5] M. C. Thompson, H. Badakov, A. M. Cook, J. B. Rosenzweig, R. Tikhoplav, G. Travish, I. Blumenfeld, M. J. Hogan, R. Ischebeck, N. Kirby, R. Siemann, D. Walz, P. Muggli, A. Scott, and R. B. Yoder, Phys. Rev. Lett. **100**, 214801 (2008).
[6] M. E. Hill, C. Adolphsen, W. Baumgartner, R. S. Callin, X. E. Lin, M. Seidel, T. Slaton, and D. H. Whittum, Phys. Rev. Lett. **87**, 094801 (2001).
[7] D. H. Whittum, SLAC Report No. SLAC-Pub-7809, 1998 (unpublished).
[8] T. P. Wangler, *RF Linear Accelerators* (John Wiley & Sons, New York, 2008).
[9] G. A. Loew, Alternate Approaches to Future Electron-Positron Linear Colliders, Stanford University, Stanford Linear Accelerator Center, CA, 1998 (unpublished).
[10] H. H. Braun, S. Döbert, I. Wilson, and W. Wuensch, Phys. Rev. Lett. **90**, 224801 (2003).
[11] G. Scheitrum, AIP Conf. Proc. **807**, 120 (2006).
[12] W. He, C. Donaldson, F. Li, L. Zhang, A. Cross, A. Phelps, K. Ronald, C. Robertson, C. Whyte, and A. Young, Int. J. Terahertz Sci. Technol. **4**, 9 (2011).
[13] W. Lawson, R. L. Ives, M. Mizuhara, J. M. Neilson, and M. E. Read, IEEE Trans. Plasma Sci., **29**, 545 (2001).
[14] H. Song, D. McDermott, Y. Hirata, L. Barnett, C. Domier, H. Hsu, T. Chang, W. Tsai, K. Chu, and N. Luhmann, Jr, Phys. Plasmas **11**, 2935 (2004).
[15] J. R. Sirigiri, M. A. Shapiro, and R. J. Temkin, Phys. Rev. Lett. **90**, 258302 (2003).
[16] K. Bane, P. Chen, and P. Wilson, IEEE Trans. Nucl. Sci. **32**, 3524 (1985).
[17] H. H. Braun, R. Corsini, T. D'Amico *et al.*, *The CLIC RF Power Source. A Novel Scheme of Two-Beam Acceleration for Electron-Positron Linear Colliders* (CERN, Geneva, Switzerland, 1999).
[18] A. Zholents, W. Gai, R. Lindberg, J. Power, Y. Sun, C. Jing, A. Kanareykin, C. Li, C. Tang, D. Shchegolkov, and E. Simakov, in *Proceedings of the 36th International Free Electron Laser Conference, Basel, Switzerland, 2014* (Genf CERN, Geneva, 2014), pp. 993–998, http://accelconf.web.cern.ch/AccelConf/FEL2014/papers/frb02.pdf.
[19] J. G. Power, W. Gai, and P. Schoessow, Phys. Rev. E **60**, 6061 (1999).
[20] C. Jing, A. Kanareykin, J. G. Power, M. Conde, Z. Yusof, P. Schoessow, and W. Gai, Phys. Rev. Lett. **98**, 144801 (2007).
[21] M. Conde, D. Doran, W. Gai, W. Liu, J. Power, C. Whiteford, E. Wisniewski, S. Antipov, C. Jing, J. Qiu, J. Shao, D. Wang, and G. Ha, in *Proceedings of IPAC2015, Richmond, VA, USA* (JACoW, 2015), p. 2472.
[22] Y. E. Sun, P. Piot, A. Johnson, A. H. Lumpkin, T. J. Maxwell, J. Ruan, and R. Thurman-Keup, Phys. Rev. Lett. **105**, 234801 (2010).
[23] P. Muggli, V. Yakimenko, M. Babzien, E. K. Kallos, and K. P. Kusche, Phys. Rev. Lett. **101**, 054801 (2008).
[24] S. Antipov, C. Jing, M. Fedurin, W. Gai, A. Kanareykin, K. Kusche, P. Schoessow, V. Yakimenko, and A. Zholents, Phys. Rev. Lett. **108**, 144801 (2012).
[25] F. Gao, M. Conde, W. Gai, C. Jing, R. Konecny, W. Liu, J. Power, T. Wong, and Z. Yusof, Phys. Rev. Accel. Beams **11**, 041301 (2008).
[26] D. Wang, S. Antipov, M. Conde, S. Doran, W. Gai, G. Ha, C. Jing, W. Liu, J. Power, J. Qiu, C. Tang, and E. Wisniewski, in *Proceedings of IPAC2015, Richmond, VA, USA* (JACoW, 2015), p. 2960.
[27] http://www.itst.ucsb.edu/?q=thomas_keating_power_meter.
[28] https://www.cst.com/products/csts2.
[29] M. Dohlus, K. Flottmann, and C. Henning, arXiv:1201.5270.
[30] W. Gai, P. Schoessow, B. Cole, R. Konecny, J. Norem, J. Rosenzweig, and J. Simpson, Phys. Rev. Lett. **61**, 2756 (1988).
[31] S. Antipov, C. Jing, A. Kanareykin, J. Butler, V. Yakimenko, M. Fedurin, K. Kusche, and W. Gai, Appl. Phys. Lett. **100**, 132910 (2012).
[32] S. Antipov, M. Babzien, C. Jing, M. Fedurin, W. Gai, A. Kanareykin, K. Kusche, V. Yakimenko, and A. Zholents, Phys. Rev. Lett. **111**, 134802 (2013).
[33] J. Power, W. Gai, X. Sun, and A. Kanareykin, in *PAC Conference Proceedings*, Vol. 1 (IEEE, 2001) pp. 114–116.
[34] C. Jing, J. Power, M. Conde, W. Liu, Z. Yusof, A. Kanareykin, and W. Gai, Phys. Rev. Accel. Beams **14**, 021302 (2011).
[35] S. Seletskiy, B. Podobedov, Y. Shen, and X. Yang, Phys. Rev. Lett. **111**, 034803 (2013).